

# Synthetic $\pi$ -flux system in 2D superconducting qubit array with tunable coupling

Yiting Liu,<sup>1,2,3,\*</sup> Jiawei Zhang,<sup>1,2,3,\*</sup> Zechen Guo,<sup>1,2,3</sup> Peisheng Huang,<sup>4,2</sup> Wenhui Huang,<sup>1,2,3</sup> Yongqi Liang,<sup>1,2,3</sup> Jiawei Qiu,<sup>1,2,3</sup> Xuandong Sun,<sup>1,2,3</sup> Zilin Wang,<sup>4,2</sup> Changrong Xie,<sup>1,2,3</sup> Xiaohan Yang,<sup>1,2,3</sup> Jiajian Zhang,<sup>1,2,3</sup> Libo Zhang,<sup>1,2,3</sup> Ji Chu,<sup>2</sup> Weijie Guo,<sup>2</sup> Ji Jiang,<sup>1,2,3</sup> Xiayu Linpeng,<sup>2</sup> Song Liu,<sup>1,2,3,5</sup> Jingjing Niu,<sup>2,5</sup> Yuxuan Zhou,<sup>2</sup> Wenhui Ren,<sup>2,†</sup> Ziyu Tao,<sup>2,‡</sup> Youpeng Zhong,<sup>1,2,3,5</sup> and Dapeng Yu<sup>1,2,3,5</sup>

<sup>1</sup>Shenzhen Institute for Quantum Science and Engineering, Southern University of Science and Technology, Shenzhen, Guangdong, China

<sup>2</sup>International Quantum Academy, Shenzhen, Guangdong, China

<sup>3</sup>Guangdong Provincial Key Laboratory of Quantum Science and Engineering, Southern University of Science and Technology, Shenzhen, Guangdong, China

<sup>4</sup>School of Physics and Electronic-Electrical Engineering, Ningxia University, Yinchuan, 750021, China

<sup>5</sup>Shenzhen Branch, Hefei National Laboratory, Shenzhen 518048, China

(Dated: January 14, 2025)

Flat-band systems provide an ideal platform for exploring exotic quantum phenomena, where the strongly suppressed kinetic energy in these flat energy bands suggests the potential for exotic phases driven by geometric structure, disorder, and interactions. While intriguing phenomena and physical mechanisms have been unveiled in theoretical models, synthesizing such systems within scalable quantum platforms remains challenging. Here, we present the experimental realization of a  $\pi$ -flux rhombic system using a two-dimensional superconducting qubit array with tunable coupling. We experimentally observe characteristic dynamics, e.g.,  $\pi$ -flux driven destructive interference, and demonstrate the protocol for eigenstate preparation in this rhombic array with coupler-assisted flux. Our results provide future possibilities for exploring the interplay of geometry, interactions, and quantum information encoding in such degenerate systems.

## INTRODUCTION

Synthetic magnetic flux in lattice structures allows effective control of their transport properties and localization behaviors [1]. For particular values of the magnetic flux, such as  $\pi$ -flux, a strong localization mechanism induced by the magnetic field can be observed in two-dimensional structures, i.e., the so-called Aharonov-Bohm (AB) caging [2–4]. These systems featuring flat energy bands are typically represented in terms of compact localized states [5–8], in which the eigenstates are strictly confined to a specific region in real space due to destructive interference [9], preventing extended transport through hopping processes. The flat bands exist in both quasi-one- and two-dimensional geometries, including the dice [8], Creutz [10], sawtooth [11], rhombic [12, 13], honeycomb [14] and Lieb lattice [15, 16]. In particular, the rhombic lattice subjected to external magnetic fields exhibits the formation of degenerate flat energy bands with localized eigenstates confined within individual unit cells, which have spurred significant theoretical and experimental advancements in condensed matter physics and quantum simulation [17–25].

Superconducting circuits have emerged as one of the promising platforms for realizing and studying lattice systems with synthetic magnetic flux [26–33]. Arrays of coupled transmon qubits can emulate complex tight-binding models providing unprecedented control over lattice geometry, on-site potentials, and inter-site couplings [34–43]. Recent experiments have demonstrated the ability to manipulate synthetic fields, enabling the realization of systems with effective magnetic flux by parametric

modulation approaches [28–32, 44], digital gates [45], and circuit design [33]. These advancements have facilitated the observation of AB caging, interaction-induced delocalization, and competition between Anderson and flat-band localization [33, 46], expanding our understanding of flat-band physics. Despite these successes, the implementation of fully controlled rhombic systems incorporating synthetic fluxes within scalable superconducting quantum circuits featuring tunable couplers remains unexplored. In this work, we experimentally realize a  $\pi$ -flux rhombic system using a superconducting circuit platform equipped with tunable couplers [47, 48]. By precisely engineering the synthetic magnetic flux assisted by tunable couplers, we achieve a highly controllable implementation of a flat-band system where the flux per plaquette can be tuned to  $\pi$ . We further illustrate the  $\pi$ -flux rhombic system with anti-symmetric detunings as another effective lattice, which enables the platforms without tunable couplings to simulate a topological trimer lattice [49, 50] or a quasiperiodic mosaic model [51]. This setup enables the exploration of a synthetic  $\pi$ -flux system with high tunability. Our results highlight the potential of superconducting circuits featuring tunable couplers for studying emergent phenomena and physical mechanisms in quantum systems with synthetic flux.

## RESULTS

### Model and experimental realization

We consider a rhombic array of superconducting qubits with tunable nearest-neighbor (NN) couplings, as illustrated in Fig. 1A, in which a synthetic flux  $\Phi = 0$  or

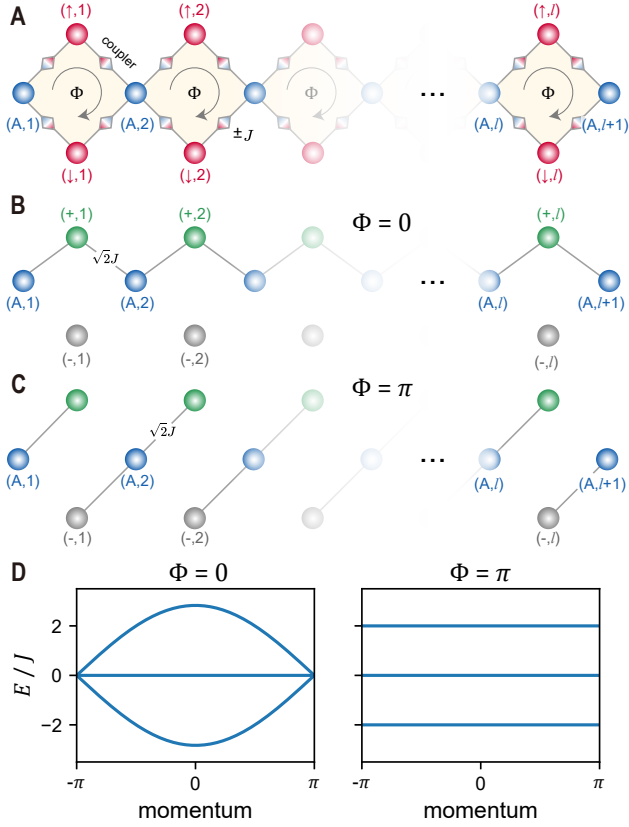


FIG. 1. (A) Schematic of the rhombic array of superconducting qubits, where the synthetic flux  $\Phi = 0$  or  $\Phi = \pi$  is controlled by tunable couplers (depicted as diamonds). (B)-(C) The effective one-dimensional model for the rhombic system: (B) with  $\Phi = 0$ , showing extended eigenstates, and (C) with  $\Phi = \pi$ , exhibiting localized eigenstates across the lattice sites in the single-excitation subspace. (D) Illustration for eigenenergy bands of the rhombic array for  $\Phi = 0$  (left) and  $\Phi = \pi$  (right) in momentum space.

$\pi$  can be effectively generated from the configuration of positive or negative coupling strengths  $\pm J$  by tunable couplers. The system can be described by the effective Hamiltonian for a rhombic lattice model with  $L = 3l + 1$  sites:

$$H/\hbar = \sum_{i,j} \Delta_{i,j} \sigma_{i,j}^+ \sigma_{i,j}^- - J \sum_{j=1}^l \left[ \sigma_{A,j}^+ (\sigma_{\uparrow,j}^- + \sigma_{\downarrow,j}^-) + \sigma_{A,j+1}^+ (\sigma_{\uparrow,j}^- + e^{i\Phi} \sigma_{\downarrow,j}^-) + \text{H.c.} \right], \quad (1)$$

where  $\sigma_{i,j}^+$  ( $\sigma_{i,j}^-$ ) represents the raising (lowering) operator for the qubit at index  $(i, j)$  with  $i \in \{A, \uparrow, \downarrow\}$  shown in Fig. 1A,  $\sigma_{i,j}^+ |0\rangle^{\otimes L} = |1_{i,j}\rangle$ ,  $\Delta_{i,j}/2\pi$  is the frequency detuning of the qubit relative to the average system frequency, and  $J$  is the homogeneous amplitude of NN coupling strengths between qubits. When  $\Phi = 0$ , achieved by configuring identical positive or negative coupling strengths and setting  $\Delta_{i,j} = 0$ , the system in the single-excitation subspace can be mapped to an effective 1D array model with coupling strengths  $\sqrt{2}J$ . In this case,

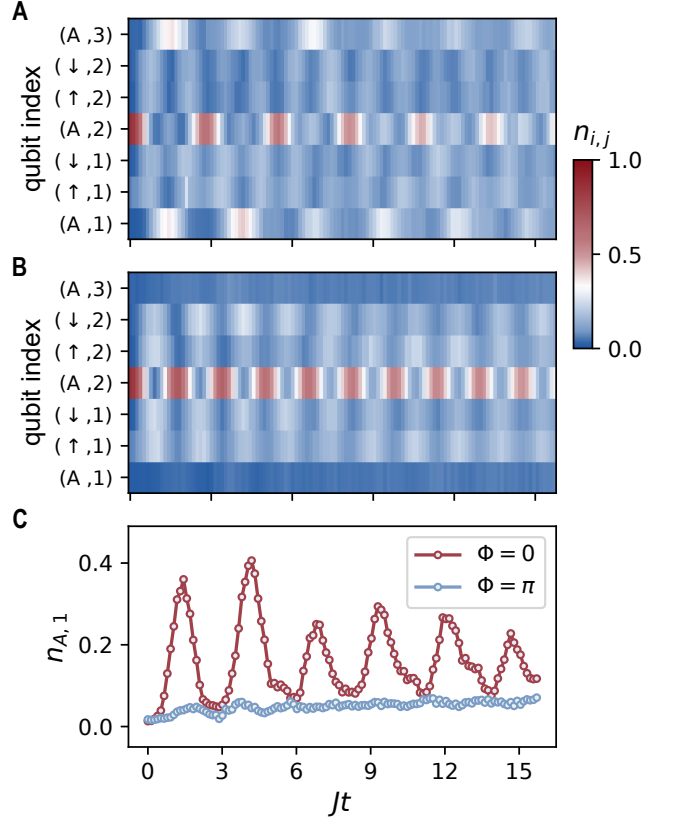


FIG. 2. **Characteristic dynamics of the rhombic array with  $\Phi = 0$  and  $\pi$ .** (A)-(B) Measured population dynamics  $n_j$  versus normalized evolution time  $Jt$  for (A)  $\Phi = 0$  and (B)  $\Phi = \pi$ . (C) Time evolution of the population for qubits located at the edge sites for  $\Phi = 0$  and  $\pi$ .

the Bell state  $|+_j\rangle = (|1_{\uparrow,j}\rangle + |1_{\downarrow,j}\rangle)/\sqrt{2}$  is regarded as a single site  $(+, j)$  in the 1D array by local unitary transformations [52], as depicted in Fig. 1B. This effective 1D array features extended dynamics with two dispersive energy bands and the states  $|-_j\rangle = (|1_{\uparrow,j}\rangle - |1_{\downarrow,j}\rangle)/\sqrt{2}$  are zero-energy eigenstates as  $H|-_j\rangle = 0$ , forming a flat band at zero energy, as shown in Fig. 1D. For  $\Phi = \pi$ , the system in the single-excitation subspace is divided into decoupled three-level (bulk) or two-level (edge) systems depicted in Fig. 1C. This configuration gives rise to an extreme localization driven by destructive interference, characterized by oscillating populations between site  $(A, j)$  and its nearest-neighboring sites [23, 46].

Here, we demonstrate the characteristic dynamics of the rhombic array consisting of  $L = 7$  qubits with effective fluxes  $\Phi = 0$  and  $\Phi = \pi$ , realized using tunable couplers in superconducting quantum circuits. As shown in Fig. 2, we present the evolution of measured population dynamics  $n_{i,j}(t) = \langle 1_{i,j} | \rho(t) | 1_{i,j} \rangle$ , for individual qubits as a function of the normalized evolution time  $Jt$  under the two flux configurations. The coupling strength is set to  $J \approx 2\pi \times 4.2$  MHz, and the system contains  $l = 2$  plaque-

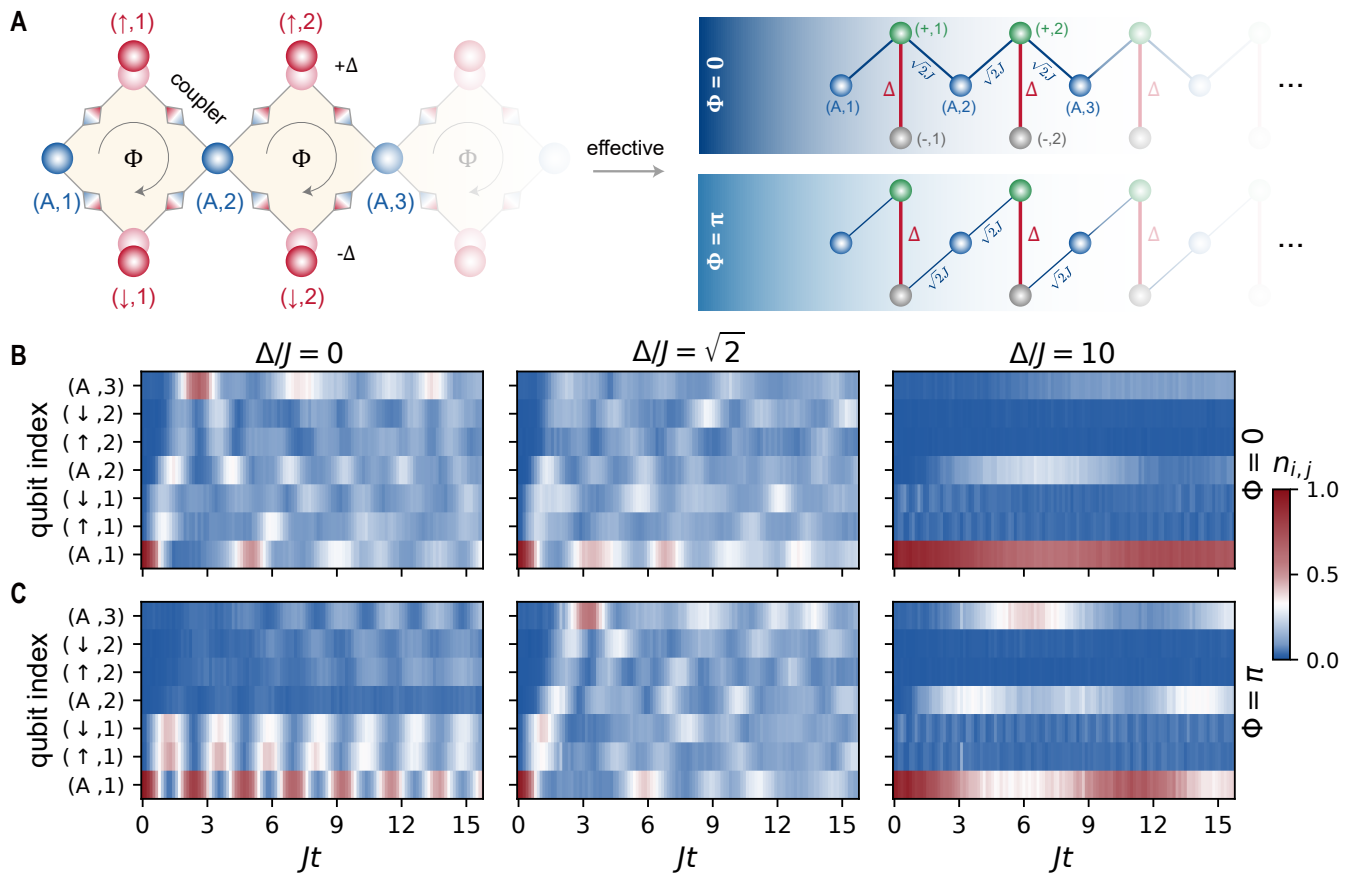


FIG. 3. **Anti-symmetric detuning on qubit frequencies.** (A) Illustration of the effective 1D model for the rhombic array with anti-symmetric detuning on qubit frequencies. In the basis of such a 1D system, the anti-symmetric detuning acts as an additional coupling, connecting the decoupled subsystems with three (two) sites in the bulk (boundary) when  $\Phi = \pi$ . (B)-(C) Measured population dynamics  $n_j$  for (B)  $\Phi = 0$  and (C)  $\Phi = \pi$ , with anti-symmetric detuning  $\Delta = 0, \sqrt{2}J$  and  $10J$ .

tes, corresponding to  $L = 7$  sites. By initially preparing the central qubit at site  $(A, 2)$  in its excited state  $|1_{A,2}\rangle$ , we examine the characteristic population dynamics of the rhombic array. For the zero-flux  $\Phi = 0$  case, we configure all coupling strengths to be negative by controlling the frequencies of the tunable couplers. The resulting population dynamics, shown in Fig. 2A, exhibit oscillations traversing all sites, consistent with the picture of an effective 1D array featuring spatially extended eigenstates (as depicted in Fig. 1B). For the  $\pi$ -flux  $\Phi = \pi$  case, we reconfigure two coupling strengths in each plaquette to be positive. The dynamics in the  $\pi$ -flux rhombic system can be interpreted as a destructive interference across each  $2 \times 2$  plaquette, where any initially localized excitation will be in a superposition of a finite number of localized eigenstates and remain bounded over time [3, 33]. In this regime, the degenerate eigenstates are localized at the site  $(A, j)$  and adjacent sites in  $\{(\uparrow, j), (\uparrow, j-1), (\downarrow, j), (\downarrow, j-1)\}$ . This localization leads to vanishing population dynamics at the edge sites  $(A, 1)$  and  $(A, 3)$  when the system is initialized in the state  $|1_{A,2}\rangle$ , as shown in Fig. 2B. Fig. 2C further illustrates the population dynamics at the

edge site  $(A, 1)$  as a function of the normalized evolution time  $Jt$  for both configurations,  $\Phi = 0$  and  $\pi$ .

### Anti-symmetric detuning

We next investigate the (de)localized dynamics by introducing anti-symmetric detunings to the qubit frequencies at sites  $(\uparrow, j)$  and  $(\downarrow, j)$ . Without detuning, the  $\pi$ -flux rhombic system hosts spatially localized eigenstates at  $(A, j)$  and its adjacent sites. These states form effective three- (two-) level systems on the bulk (edge) sites in the basis of  $|\pm_j\rangle = (|1_{\uparrow,j}\rangle \pm |1_{\downarrow,j}\rangle)/\sqrt{2}$  and  $|1_{A,j}\rangle$  as shown in Fig. 1C. The anti-symmetric detunings on the qubit frequencies act as  $\Delta\sigma_{\uparrow,j}^+\sigma_{\uparrow,j}^-$  and  $-\Delta\sigma_{\downarrow,j}^+\sigma_{\downarrow,j}^-$  in the basis of  $|1_{\uparrow,j}\rangle$  and  $|1_{\downarrow,j}\rangle$ , respectively, introducing effective couplings between the states  $|\pm_j\rangle$ . This is consistent with the delocalization of the  $\pi$ -flux rhombus when anti-symmetric on-site disorders are introduced [23, 46]. In the  $\pi$ -flux rhombic array with anti-symmetric detuning  $\Delta = \sqrt{2}J$ , the system can be described by an effective 1D model on the sites  $(A, 1), (+, 1), (-, 1), (A, 2), (+, 1) \dots$  with homogeneous couplings  $\sqrt{2}J$ , as illustrated in Fig. 3A. For a general value of anti-symmetric

detuning  $\Delta$ , this  $\pi$ -flux system can be effectively represented by a trimer lattice [49, 50] with intra-cell couplings  $\sqrt{2}J$  controlled by the tunable couplers and inter-cell couplings  $\Delta$  determined by the anti-symmetric detunings on the qubit frequencies, where the unit cell is defined on the sites  $\{(-, j-1), (A, j), (+, j)\}$ . According to previous theoretical studies [49], the topological properties of this trimer lattice are regulated by the relative strengths of the inter-cell and intra-cell coupling amplitudes, where the Zak phase is found to be  $\mathcal{Z} = \pi$  ( $\mathcal{Z} = 0$ ) for  $\Delta > \sqrt{2}J$  ( $\Delta < \sqrt{2}J$ ) corresponding to the (non-) topological phase of the trimer lattice [49, 50].

We experimentally investigate a coupler-assisted rhombic system with anti-symmetric detunings on the qubit frequencies in  $l = 2$  plaquettes with  $L = 7$  sites. A single-particle excitation is initialized at the edge site  $(A, 1)$ , and the population dynamics of each site are tracked over normalized time  $Jt$ , as shown in Fig. 3 (B and C). In the absence of anti-symmetric detuning  $\Delta = 0$ , the zero-flux rhombic system exhibits extended population dynamics across all sites, while the  $\pi$ -flux rhombic system demonstrates oscillatory, localized dynamics confined to the sites  $\{(A, 1), (\uparrow, 1), (\downarrow, 1)\}$ . When the anti-symmetric detuning is involved, the dynamics of the zero-flux system become less extended, whereas the  $\pi$ -flux system exhibits increased delocalization compared to the detuning-free counterpart, which can be effectively described using a comb-like and trimer lattice model shown in Fig. 3A. For a larger detuning  $\Delta = 10J$ , the localized behavior in the zero-flux rhombic system is further enhanced, as presented in Fig. 3B. In contrast, the  $\pi$ -flux system (Fig. 3C) demonstrates population dynamics that traverse the middle site  $(A, j)$  of the unit cell in the trimer lattice due to the sizeable inter-cell couplings [49, 50]. Numerical simulations supporting these observations are provided in the Supplemental Material.

### Ground state preparation

We further investigate the energy spectrum and ground state of the minimal  $\pi$ -flux rhombic system comprising  $L = 4$  qubits. To unveil the energy spectrum, we perform a spectroscopy measurement on the qubit  $Q_{A,1}$  by applying a driving pulse through XY control line while keeping the qubit frequencies on resonance  $\Delta_{i,j} = 0$  and setting the coupling strengths according to the Hamiltonian in Eq. (1). In this spectroscopy, an increase in the measured population indicates that the applied pump tone is in resonance with one of the eigenfrequencies of the rhombic system, giving a transition from  $|0\rangle^{\otimes L}$  to the eigenstates in the single-excitation subspace [33, 53]. As shown in Fig. 4A, the spectroscopy reveals two population peaks corresponding to the eigenenergies  $E = \sqrt{2}J$  and  $-\sqrt{2}J$  for  $\pi$ -flux  $\Phi = \pi$ .

We employ an adiabatic protocol to prepare the ground state of  $\pi$ -flux rhombic system [44, 54]. The system is initialized in a simple ground state  $|1_{A,1}\rangle$  where the ex-

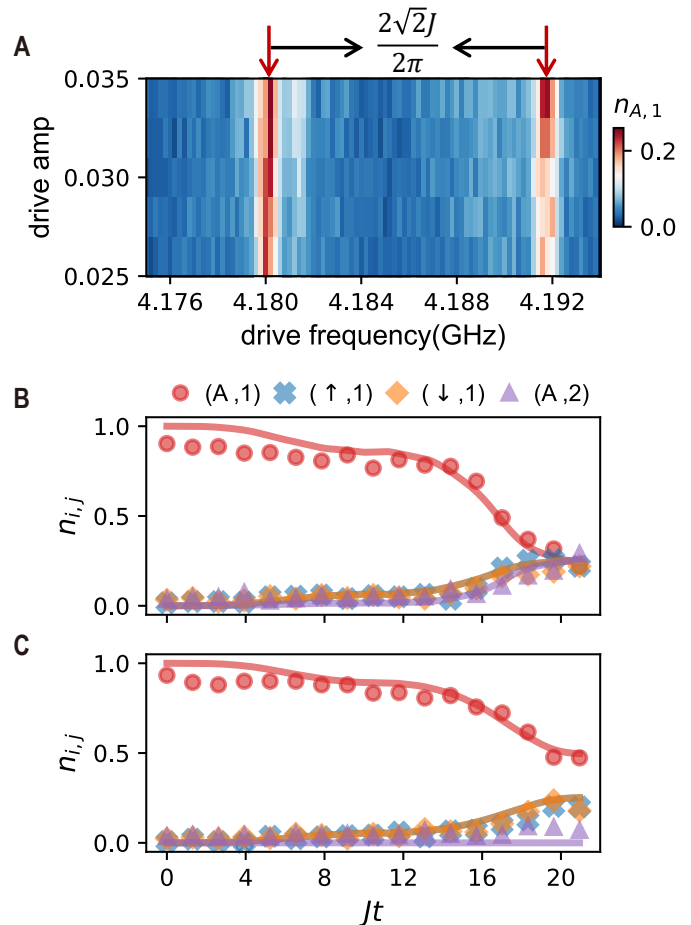


FIG. 4. **Energy spectrum and ground state preparation of the rhombic system.** (A) Spectroscopy of the  $\pi$ -flux rhombic array with four superconducting qubits ( $Q_{A,1}$ ,  $Q_{\uparrow,1}$ ,  $Q_{\downarrow,1}$ ,  $Q_{A,2}$ ), in which the increased population peaks indicate the eigenenergies of this system. (B)-(C) The measured population during the adiabatic preparation of the ground state for the rhombic system from the initial state  $|1_{A,1}\rangle$ , where (B)  $\Phi = 0$ , (C)  $\Phi = \pi$ . Dots indicate measured results, while solid lines denote the corresponding numerical simulation.

citation is localized at the site  $(A, 1)$ . The frequency of this site is primarily detuned ( $|\Delta_{A,1}|/J > 3$ ) below the other qubit frequencies, and the couplings are turned off ( $J = 0$ ). Then we gradually evolve the system by ramping up the couplings to  $J \approx 2\pi \times 4.2$  MHz and successively ramping down the detuning frequency to reach the final Hamiltonian of the rhombic system with  $\Delta_{i,j} = 0$ . As shown in Fig. 4 (B and C), the rhombic system follows the instantaneous ground state during the slow adiabatic evolution, reaching the ground state with (un)equally distributed population on each site measured for  $\Phi = 0$  ( $\Phi = \pi$ ), consistent with the results calculated in numerical simulation.

### DISCUSSION

In this work, we experimentally realize a synthetic  $\pi$ -flux rhombic system using tunable couplers in superconducting quantum circuits. By properly configuring the positive or negative coupling strengths between neighboring qubits by tunable couplers, we demonstrate the characteristic dynamics of a rhombic array of superconducting qubits with synthetic flux  $\Phi = 0$  and  $\pi$ . We illustrate that the dynamics of  $\pi$ -flux rhombic system with anti-symmetric detunings can be effectively described by a trimer lattice in specific bases, and demonstrate the system dynamics with different detunings acting as inter-cell couplings in the effective trimer lattice. Such equivalent representation deepens our understanding of flat-band physics in the  $\pi$ -flux rhombic system [52], and provides the possibility for the experimental platforms without tunable coupling strengths to simulate a topological trimer lattice [49, 50] or quasiperiodic mosaic model [51] whose inter-cell couplings can be effectively controlled by the on-site detunings in real space. Using the adiabatic protocol, we further demonstrate the ground state preparation in such a rhombic system by ramping up the tunable couplings' strengths and adjusting the qubit frequencies. Utilizing the synthetic  $\pi$ -flux system with high tunability, further efforts can be made to explore the quantum information encoding of the eigenstates in such degenerate system [55] according to the similar protocols in recently developed dual-rail qubits [56–60].

**Acknowledgments:** This work was supported by the Shenzhen Science and Technology Program (Grant No. RCBS20231211090824040), the National Natural Science Foundation of China (12204228, 12374474), the Innovation Program for Quantum Science and Technology (2021ZD0301703), the Shenzhen-Hong Kong Cooperation Zone for Technology and Innovation (HZQB-KCZYB-2020050), and Guangdong Basic and Applied Basic Research Foundation (2024A1515011714, 2022A1515110615).

**Competing interests:** The authors declare no conflict of interest.

---

\* These authors contributed equally to this work

† [renwenhui@iqasz.cn](mailto:renwenhui@iqasz.cn)

‡ [taoziyu@iqasz.cn](mailto:taoziyu@iqasz.cn)

- [1] J. Dalibard, F. Gerbier, G. Juzeliūnas, and P. Öhberg, *Colloquium: Artificial gauge potentials for neutral atoms*, *Rev. Mod. Phys.* **83**, 1523 (2011).
- [2] Y. Aharonov and D. Bohm, *Significance of electromagnetic potentials in the quantum theory*, *Phys. Rev.* **115**, 485 (1959).
- [3] J. Vidal, R. Mosseri, and B. Douçot, *Aharonov-Bohm cages in two-dimensional structures*, *Phys. Rev. Lett.* **81**, 5888 (1998).
- [4] J. Vidal, B. Douçot, R. Mosseri, and P. Butaud, *Interaction induced delocalization for two particles in a periodic potential*, *Phys. Rev. Lett.* **85**, 3906 (2000).
- [5] D. L. Bergman, C. Wu, and L. Balents, *Band touching from real-space topology in frustrated hopping models*, *Phys. Rev. B* **78**, 125104 (2008).
- [6] S. Flach, D. Leykam, J. D. Bodyfelt, P. Matthies, and A. S. Desyatnikov, *Detangling flat bands into Fano lattices*, *Europhys. Lett.* **105**, 30001 (2014).
- [7] W. Maimaiti, S. Flach, and A. Andreanov, *Universal  $d = 1$  flat band generator from compact localized states*, *Phys. Rev. B* **99**, 125129 (2019).
- [8] S. M. Zhang and L. Jin, *Compact localized states and localization dynamics in the dice lattice*, *Phys. Rev. B* **102**, 054301 (2020).
- [9] J.-W. Rhim and B.-J. Yang, *Classification of flat bands according to the band-crossing singularity of Bloch wave functions*, *Phys. Rev. B* **99**, 045107 (2019).
- [10] Y. He, R. Mao, H. Cai, J.-X. Zhang, Y. Li, L. Yuan, S.-Y. Zhu, and D.-W. Wang, *Flat-band localization in Creutz superradiance lattices*, *Phys. Rev. Lett.* **126**, 103601 (2021).
- [11] W. Maimaiti, A. Andreanov, H. C. Park, O. Gendelman, and S. Flach, *Compact localized states and flat-band generators in one dimension*, *Phys. Rev. B* **95**, 115135 (2017).
- [12] C. E. Creffield and G. Platero, *Coherent control of interacting particles using dynamical and Aharonov-Bohm phases*, *Phys. Rev. Lett.* **105**, 086804 (2010).
- [13] A. Bermudez, T. Schaetz, and D. Porras, *Synthetic gauge fields for vibrational excitations of trapped ions*, *Phys. Rev. Lett.* **107**, 150501 (2011).
- [14] C. Wu, D. Bergman, L. Balents, and S. Das Sarma, *Flat bands and Wigner crystallization in the honeycomb optical lattice*, *Phys. Rev. Lett.* **99**, 070401 (2007).
- [15] E. H. Lieb, *Two theorems on the Hubbard model*, *Phys. Rev. Lett.* **62**, 1201 (1989).
- [16] A. Julku, S. Peotta, T. I. Vanhala, D.-H. Kim, and P. Törmä, *Geometric origin of superfluidity in the Lieb-lattice flat band*, *Phys. Rev. Lett.* **117**, 045303 (2016).
- [17] S. Sugawa, F. Salces-Carcoba, A. R. Perry, Y. Yue, and I. B. Spielman, *Second Chern number of a quantum-simulated non-Abelian Yang monopole*, *Science* **360**, 1429 (2018).
- [18] S. Mukherjee, M. Di Liberto, P. Öhberg, R. R. Thomson, and N. Goldman, *Experimental observation of Aharonov-Bohm cages in photonic lattices*, *Phys. Rev. Lett.* **121**, 075502 (2018).
- [19] M. Di Liberto, S. Mukherjee, and N. Goldman, *Nonlinear dynamics of Aharonov-Bohm cages*, *Phys. Rev. A* **100**, 043829 (2019).
- [20] M. Kremer, I. Petrides, E. Meyer, M. Heinrich, O. Zilberberg, and A. Szameit, *A square-root topological insulator with non-quantized indices realized with photonic Aharonov-Bohm cages*, *Nat. Commun.* **11**, 907 (2020).
- [21] S. Longhi, *Inverse Anderson transition in photonic cages*, *Opt. Lett.* **46**, 2872 (2021).
- [22] G. Cáceres-Aravena, D. Guzmán-Silva, I. Salinas, and R. A. Vicencio, *Controlled transport based on multiorbital Aharonov-Bohm photonic caging*, *Phys. Rev. Lett.* **128**, 256602 (2022).
- [23] H. Li, Z. Dong, S. Longhi, Q. Liang, D. Xie, and B. Yan, *Aharonov-Bohm caging and inverse Anderson transition in ultracold atoms*, *Phys. Rev. Lett.* **129**, 220403 (2022).
- [24] S. Maity, B. Paul, S. P. Sharma, and T. Mishra, *Dynamics of interacting particles on a rhombus chain*:

- Aharonov-Bohm caging and inverse Anderson transition*, [arXiv preprint, arXiv:2409.05853](#) (2024).
- [25] E. Nicolau, A. M. Marques, R. G. Dias, J. Mompert, and V. Ahufinger, *Many-body Aharonov-Bohm caging in a lattice of rings*, *Phys. Rev. A* **107**, 023305 (2023).
- [26] A. Vepsäläinen, S. Danilin, and G. S. Paraoanu, *Superadiabatic population transfer in a three-level superconducting circuit*, *Sci. Adv.* **5**, 2 (2019).
- [27] A. Vepsäläinen and G. S. Paraoanu, *Simulating spin chains using a superconducting circuit: Gauge invariance, superadiabatic transport, and broken time-reversal symmetry*, *Adv. Quantum Technol.* **3**, 4 (2020).
- [28] I. T. Rosen, S. Muschinske, C. N. Barrett, A. Chatterjee, M. Hays, M. A. DeMarco, A. H. Karamlou, D. A. Rower, R. Das, D. K. Kim, B. M. Niedzielski, M. Schuldt, K. Serniak, M. E. Schwartz, J. L. Yoder, J. A. Grover, and W. D. Oliver, *A synthetic magnetic vector potential in a 2d superconducting qubit array*, *Nat. Phys.* **20**, 1881 (2024).
- [29] P. Roushan, C. Neill, A. Megrant, Y. Chen, R. Babush, R. Barends, B. Campbell, Z. Chen, B. Chiaro, A. Dunsworth, *et al.*, *Chiral ground-state currents of interacting photons in a synthetic magnetic field*, *Nat. Phys.* **13**, 146 (2016).
- [30] D.-W. Wang, C. Song, W. Feng, H. Cai, D. Xu, H. Deng, H. Li, D. Zheng, X. Zhu, H. Wang, S.-Y. Zhu, and M. O. Scully, *Synthesis of antisymmetric spin exchange interaction and chiral spin clusters in superconducting circuits*, *Nat. Phys.* **15**, 382 (2019).
- [31] W. Liu, W. Feng, W. Ren, D.-W. Wang, and H. Wang, *Synthesizing three-body interaction of spin chirality with superconducting qubits*, *Appl. Phys. Lett.* **116**, 114001 (2020).
- [32] J. Zhang, W. Huang, J. Chu, J. Qiu, X. Sun, Z. Tao, J. Zhang, L. Zhang, Y. Zhou, Y. Chen, Y. Liu, S. Liu, Y. Zhong, J.-J. Miao, J. Niu, and D. Yu, *Synthetic multi-dimensional Aharonov-Bohm cages in Fock state lattices*, [arXiv preprint, arXiv:2412.09766](#) (2024).
- [33] J. G. C. Martinez, C. S. Chiu, B. M. Smitham, and A. A. Houck, *Flat-band localization and interaction-induced delocalization of photons*, *Sci. Adv.* **9**, 50 (2023).
- [34] Z. Yan, Y.-R. Zhang, M. Gong, Y. Wu, Y. Zheng, S. Li, C. Wang, F. Liang, J. Lin, Y. Xu, C. Guo, L. Sun, C.-Z. Peng, K. Xia, H. Deng, H. Rong, J. Q. You, F. Nori, H. Fan, X. Zhu, and J.-W. Pan, *Strongly correlated quantum walks with a 12-qubit superconducting processor*, *Science* **364**, 753 (2019).
- [35] R. Ma, B. Saxberg, C. Owens, N. Leung, Y. Lu, J. Simon, and D. I. Schuster, *A dissipatively stabilized Mott insulator of photons*, *Nature* **566**, 51 (2019).
- [36] J. Deng, H. Dong, C. Zhang, Y. Wu, J. Yuan, X. Zhu, F. Jin, H. Li, Z. Wang, H. Cai, C. Song, H. Wang, J. Q. You, and D.-W. Wang, *Observing the quantum topology of light*, *Science* **378**, 966 (2022).
- [37] A. H. Karamlou, J. Braumüller, Y. Yanay, A. Di Paolo, P. M. Harrington, B. Kannan, D. Kim, M. Kjaergaard, A. Melville, S. Muschinske, *et al.*, *Quantum transport and localization in 1d and 2d tight-binding lattices*, *npj Quantum Inf.* **8**, 35 (2022).
- [38] Y. Yao, L. Xiang, Z. Guo, Z. Bao, Y.-F. Yang, Z. Song, H. Shi, X. Zhu, F. Jin, J. Chen, *et al.*, *Observation of many-body Fock space dynamics in two dimensions*, *Nat. Phys.* **19**, 1459 (2023).
- [39] A. H. Karamlou, I. T. Rosen, S. E. Muschinske, C. N. Barrett, A. Di Paolo, L. Ding, P. M. Harrington, M. Hays, R. Das, D. K. Kim, B. M. Niedzielski, M. Schuldt, K. Serniak, M. E. Schwartz, J. L. Yoder, S. Gustavsson, Y. Yanay, J. A. Grover, and W. D. Oliver, *Probing entanglement in a 2d hard-core Bose-Hubbard lattice*, *Nature* **629**, 561 (2024).
- [40] Y.-H. Shi, Z.-H. Sun, Y.-Y. Wang, Z.-A. Wang, Y.-R. Zhang, W.-G. Ma, H.-T. Liu, K. Zhao, J.-C. Song, G.-H. Liang, Z.-Y. Mei, J.-C. Zhang, H. Li, C.-T. Chen, X. Song, J. Wang, G. Xue, H. Yu, K. Huang, Z. Xiang, K. Xu, D. Zheng, and H. Fan, *Probing spin hydrodynamics on a superconducting quantum simulator*, *Nat. Commun.* **15**, 7573 (2024).
- [41] L. Xiang, J. Chen, Z. Zhu, Z. Song, Z. Bao, X. Zhu, F. Jin, K. Wang, S. Xu, Y. Zou, H. Li, Z. Wang, C. Song, A. Yue, J. Partridge, Q. Guo, R. Mondaini, H. Wang, and R. T. Scalettar, *Enhanced quantum state transfer by circumventing quantum chaotic behavior*, *Nat. Commun.* **15**, 4918 (2024).
- [42] C.-L. Deng, Y. Liu, Y.-R. Zhang, X.-G. Li, T. Liu, C.-T. Chen, T. Liu, C.-W. Lu, Y.-Y. Wang, T.-M. Li, C.-P. Fang, S.-Y. Zhou, J.-C. Song, Y.-S. Xu, Y. He, Z.-H. Liu, K.-X. Huang, Z.-C. Xiang, J.-C. Wang, D.-N. Zheng, G.-M. Xue, K. Xu, H.-F. Yu, and H. Fan, *High-order topological pumping on a superconducting quantum processor*, *Phys. Rev. Lett.* **133**, 140402 (2024).
- [43] Y. Liu, Y.-R. Zhang, Y.-H. Shi, T. Liu, C. Lu, Y.-Y. Wang, H. Li, T.-M. Li, C.-L. Deng, S.-Y. Zhou, T. Liu, J.-C. Zhang, G.-H. Liang, Z.-Y. Mei, W.-G. Ma, H.-T. Liu, Z.-H. Liu, C.-T. Chen, K. Huang, X. Song, S. P. Zhao, Y. Tian, Z. Xiang, D. Zheng, F. Nori, K. Xu, and H. Fan, *Interplay between disorder and topology in Thouless pumping on a superconducting quantum processor*, *Nat. Commun.* **16**, 108 (2025).
- [44] C. Wang, F.-M. Liu, M.-C. Chen, H. Chen, X.-H. Zhao, C. Ying, Z.-X. Shang, J.-W. Wang, Y.-H. Huo, C.-Z. Peng, X. Zhu, C.-Y. Lu, and J.-W. Pan, *Realization of fractional quantum Hall state with interacting photons*, *Science* **384**, 579 (2024).
- [45] C. Neill, T. McCourt, X. Mi, Z. Jiang, M. Y. Niu, W. Mruzckiewicz, I. Aleiner, F. Arute, K. Arya, J. Atalaya, *et al.*, *Accurately computing the electronic properties of a quantum ring*, *Nature* **594**, 508 (2021).
- [46] I. T. Rosen, S. Muschinske, C. N. Barrett, D. A. Rower, R. Das, D. K. Kim, B. M. Niedzielski, M. Schuldt, K. Serniak, M. E. Schwartz, J. L. Yoder, J. A. Grover, and W. D. Oliver, *Flat-band (de)localization emulated with a superconducting qubit array*, [arXiv preprint, arXiv:2410.07878](#) (2024).
- [47] F. Yan, P. Krantz, Y. Sung, M. Kjaergaard, D. L. Campbell, T. P. Orlando, S. Gustavsson, and W. D. Oliver, *Tunable coupling scheme for implementing high-fidelity two-qubit gates*, *Phys. Rev. Applied* **10**, 054062 (2018).
- [48] Y. Xu, J. Chu, J. Yuan, J. Qiu, Y. Zhou, L. Zhang, X. Tan, Y. Yu, S. Liu, J. Li, *et al.*, *High-fidelity, high-scalability two-qubit gate scheme for superconducting qubits*, *Phys. Rev. Lett.* **125**, 240503 (2020).
- [49] V. M. Martinez Alvarez and M. D. Coutinho-Filho, *Edge states in trimer lattices*, *Phys. Rev. A* **99**, 013833 (2019).
- [50] A. Anastasiadis, G. Styliaris, R. Chaunsali, G. Theocharis, and F. K. Diakonou, *Bulk-edge correspondence in the trimer Su-Schrieffer-Heeger model*, *Phys. Rev. B* **106**, 085109 (2022).
- [51] X.-C. Zhou, Y. Wang, T.-F. J. Poon, Q. Zhou, and X.-J.

- Liu, *Exact new mobility edges between critical and localized states*, *Phys. Rev. Lett.* **131**, 176401 (2023).
- [52] C. Danieli, A. Andreanov, T. Mithun, and S. Flach, *Non-linear caging in all-bands-flat lattices*, *Phys. Rev. B* **104**, 085131 (2021).
- [53] S. N. M. Paladugu, T. Chen, F. A. An, B. Yan, and B. Gadway, *Injection spectroscopy of momentum state lattices*, *Commun. Phys.* **7**, 39 (2024).
- [54] B. Saxberg, A. Vrajitoarea, G. Roberts, M. G. Panetta, J. Simon, and D. I. Schuster, *Disorder-assisted assembly of strongly correlated fluids of light*, *Nature* **612**, 435 (2022).
- [55] M. Röntgen, C. Morfonios, I. Brouzos, F. Diakonov, and P. Schmelcher, *Quantum network transfer and storage with compact localized states induced by local symmetries*, *Phys. Rev. Lett.* **123**, 080504 (2019).
- [56] D. L. Campbell, Y.-P. Shim, B. Kannan, R. Winik, D. K. Kim, A. Melville, B. M. Niedzielski, J. L. Yoder, C. Tahan, S. Gustavsson, and W. D. Oliver, *Universal nonadiabatic control of small-gap superconducting qubits*, *Phys. Rev. X* **10**, 041051 (2020).
- [57] J. D. Teoh, P. Winkel, H. K. Babla, B. J. Chapman, J. Claes, S. J. de Graaf, J. W. O. Garmon, W. D. Kalfus, Y. Lu, A. Maiti, K. Sahay, N. Thakur, T. Tsunoda, S. H. Xue, L. Frunzio, S. M. Girvin, S. Puri, and R. J. Schoelkopf, *Dual-rail encoding with superconducting cavities*, *Proc. Natl. Acad. Sci.* **120**, 41 (2023).
- [58] K. S. Chou, T. Shemma, H. McCarrick, T.-C. Chien, J. D. Teoh, P. Winkel, A. Anderson, J. Chen, J. C. Curtis, S. J. de Graaf, *et al.*, *A superconducting dual-rail cavity qubit with erasure-detected logical measurements*, *Nat. Phys.* **20**, 1454 (2024).
- [59] H. Levine, A. Haim, J. Hung, N. Alidoust, M. Kalae, L. DeLorenzo, E. Wollack, P. Arrangoiz-Arriola, A. Khalajhedayati, R. Sanil, *et al.*, *Demonstrating a long-coherence dual-rail erasure qubit using tunable transmons*, *Phys. Rev. X* **14**, 011051 (2024).
- [60] A. Koottandavida, I. Tsioutsios, A. Kargioti, C. R. Smith, V. R. Joshi, W. Dai, J. D. Teoh, J. C. Curtis, L. Frunzio, R. J. Schoelkopf, and M. H. Devoret, *Erasure detection of a dual-rail qubit encoded in a double-post superconducting cavity*, *Phys. Rev. Lett.* **132**, 180601 (2024).

# Supplementary Material for “Synthetic $\pi$ -flux system in 2D superconducting qubit array with tunable coupling”

## CONTENTS

I. Details on theoretical model	2
II. Experiment	3
A. Device information	3
B. Experimental realization and numerical simulation	3
References	7



## I. DETAILS ON THEORETICAL MODEL

The system discussed in the main text can be described by an effective Hamiltonian of a rhombic lattice model with  $L = 3l + 1$  sites ( $l$  is the number of rhombic plaquettes) [1–4]:

$$H/\hbar = \sum_{i,j} \Delta_{i,j} \sigma_{i,j}^+ \sigma_{i,j}^- - J \sum_{j=1}^l [\sigma_{A,j}^+ (\sigma_{\uparrow,j}^- + \sigma_{\downarrow,j}^-) + \sigma_{A,j+1}^+ (\sigma_{\uparrow,j}^- + e^{i\Phi} \sigma_{\downarrow,j}^-) + \text{H.c.}], \quad (\text{S1})$$

where  $\sigma_{i,j}^+$  ( $\sigma_{i,j}^-$ ) represents the raising (lowering) operator for the qubit at site  $(i, j)$  with  $i \in \{A, \uparrow, \downarrow\}$ ,  $\sigma_{i,j}^+ |0\rangle^{\otimes L} = |1_{i,j}\rangle$ ,  $\Delta_{i,j}/2\pi$  is the detuning of the qubit relative to the average system frequency, and  $J$  is the homogeneous amplitude of NN coupling strengths between qubits.

When the system is configured as  $\Phi = 0$  by using the same negative coupling strengths and  $\Delta_{i,j} = 0$ , the effective Hamiltonian in the single-excitation subspace can be written in the form of one-dimensional (1D) array:

$$H_{\Phi=0}/\hbar = -\sqrt{2}J \sum_{j=1}^l (\sigma_{A,j}^+ \sigma_{+,j}^- + \sigma_{A,j+1}^+ \sigma_{+,j}^- + \text{H.c.}), \quad (\text{S2})$$

where  $\sigma_{+,j}^+ = (\sigma_{\uparrow,j}^+ + \sigma_{\downarrow,j}^+)/\sqrt{2}$ ,  $\sigma_{-,j}^+ = (\sigma_{\uparrow,j}^+ - \sigma_{\downarrow,j}^+)/\sqrt{2}$ . In this representation, the Bell state  $|+_j\rangle = (|1_{\uparrow,j}\rangle + |1_{\downarrow,j}\rangle)/\sqrt{2}$  forms an effective 1D array on the  $2l + 1$  sites  $\{(A, 1), (+, 1), (A, 2), (+, 2), \dots\}$  in the single-excitation subspace [5]. Besides the effective 1D array featuring two dispersive energy bands, the Bell state  $|-_j\rangle = (|1_{\uparrow,j}\rangle - |1_{\downarrow,j}\rangle)/\sqrt{2}$  is decoupled with the system Hamiltonian,  $H|-_j\rangle = 0$ , resulting in a flat band with zero eigenenergies.

In another scenario of  $\Phi = \pi$ , the effective Hamiltonian in the single-excitation subspace can be written as:

$$H_{\Phi=\pi}/\hbar = -\sqrt{2}J \sum_{j=1}^l (\sigma_{A,j}^+ \sigma_{+,j}^- + \sigma_{A,j+1}^+ \sigma_{-,j}^- + \text{H.c.}). \quad (\text{S3})$$

This yields decoupled three-level systems in the bulk sites  $\{(-, j-1), (A, j), (+, j)\}$ , and two-level systems in the edge sites  $\{(A, 0), (+, 0)\}$  and  $\{(-, l), (A, l+1)\}$ .

Introducing the anti-symmetric detunings ( $\Delta_{\uparrow,j} = \Delta$  and  $\Delta_{\downarrow,j} = -\Delta$ ) on the qubit, the system can be described by the Hamiltonian

$$H/\hbar = \sum_j \Delta (\sigma_{\uparrow,j}^+ \sigma_{\uparrow,j}^- - \sigma_{\downarrow,j}^+ \sigma_{\downarrow,j}^-) - J \sum_{j=1}^l [\sigma_{A,j}^+ (\sigma_{\uparrow,j}^- + \sigma_{\downarrow,j}^-) + \sigma_{A,j+1}^+ (\sigma_{\uparrow,j}^- \pm \sigma_{\downarrow,j}^-) + \text{H.c.}]. \quad (\text{S4})$$

In the basis  $|\pm_j\rangle = (|1_{\uparrow,j}\rangle \pm |1_{\downarrow,j}\rangle)/\sqrt{2}$ , the Hamiltonian can be written as

$$H/\hbar = \sum_{j=1}^l \left[ \Delta \sigma_{+,j}^+ \sigma_{-,j}^- - \sqrt{2}J (\sigma_{A,j}^+ \sigma_{+,j}^- + \sigma_{A,j+1}^+ \sigma_{\pm,j}^-) + \text{H.c.} \right], \quad (\text{S5})$$

which gives additional coupling between the states  $|1_{+,j}\rangle$  and  $|1_{-,j}\rangle$ . For the  $\Phi = \pi$  rhombic system, the anti-symmetric detunings induce inter-cell couplings between the effective unit cell of three-level systems, comprising the states  $\{|1_{-,j-1}\rangle, |1_{A,j}\rangle, |1_{+,j}\rangle\}$  localized in the bulk sites, and two-level systems with states  $\{|1_{A,0}\rangle, |1_{+,0}\rangle\}$  or  $\{|1_{-,l}\rangle, |1_{A,l+1}\rangle\}$  localized at the edge sites. Consequently, the  $\pi$ -flux system with anti-symmetric detunings can be effectively mapped onto a 1D trimer lattice [6, 7], characterized by intra-cell couplings of  $\sqrt{2}J$  and inter-cell couplings of  $\Delta$ .

## II. EXPERIMENT

### A. Device information

Our experiment is performed on a  $6 \times 11$  square-lattice quantum processor using tunable coupling scheme [8, 9], which shares the same overall design as described in Ref. [10]. The effective coupling strength between two neighboring qubits is tunable within a range of about +5 MHz to -20 MHz. In this study, we utilize 7 (or 4) qubits to construct rhombic plaquettes for investigating quantum properties. These qubits are labeled as  $Q_{i,j}$  ( $i = A, \uparrow, \downarrow$  and  $j = 1, 2$ ). The detailed characterization parameters of these qubits are provided in Table. S1.

### B. Experimental realization and numerical simulation

We investigate the characteristic population dynamics for  $L = 7$  qubits under sequential excitation. Specifically, we present the results for excitation at the sites  $(A, 1)$ ,  $(\uparrow, 1)$ ,  $(\downarrow, 1)$ ,  $(\uparrow, 2)$ ,  $(\downarrow, 2)$  and  $(A, 3)$ , respectively, in addition to the previously shown excitation at the site  $(A, 2)$  in Fig. 2 of the main text. The experimental results and corresponding numerical simulations are presented in Fig. S1 with effective fluxes  $\Phi = 0$  and  $\Phi = \pi$ , using the same coupling strength and the normalized evolution time.

The (de)localized dynamics induced by adding anti-symmetric detunings,  $\Delta$  and  $-\Delta$ , to

Table S1. **Qubits properties.**  $\omega_{\min}/2\pi$  ( $\omega_{\max}/2\pi$ ) is the qubit sweet point and  $\omega_{\text{idle}}/2\pi$  is the qubit idle frequency.  $T_{1,\text{idle}}$  is the qubit relaxation time measured at idle frequency.  $T_{2,\phi}$  denotes the qubit dephasing time.  $F_0$  and  $F_1$  are the readout fidelities of qubit  $|0\rangle$  state and  $|1\rangle$  state, respectively.

	$Q_{A,1}$	$Q_{\uparrow,1}$	$Q_{\downarrow,1}$	$Q_{A,2}$	$Q_{\uparrow,2}$	$Q_{\downarrow,2}$	$Q_{A,3}$
$\omega_{\min}/2\pi$ (GHz)	3.639	3.816	3.972	3.795	3.909	3.952	3.898
$\omega_{\max}/2\pi$ (GHz)	4.891	4.867	5.055	5.121	5.109	5.217	5.083
$\omega_{\text{idle}}/2\pi$ (GHz)	4.120	4.160	4.239	4.208	4.110	4.165	4.231
$\omega_r/2\pi$ (GHz)	6.216	6.112	6.118	6.160	6.186	6.190	6.083
$T_{1,\text{idle}}$ ( $\mu\text{s}$ )	63.7	68.4	54.0	40.0	55.6	42.8	68.8
$T_{2,\phi}$ ( $\mu\text{s}$ )	9.7	12.8	9.8	3.8	12.8	8.4	10.8
$F_0$	0.983	0.976	0.972	0.990	0.987	0.989	0.975
$F_1$	0.973	0.972	0.965	0.962	0.940	0.972	0.972

the qubits at the sites  $(\uparrow, j)$  and  $(\downarrow, j)$ , respectively, is realized through additional z pulses that adjust the frequencies of the target qubits. Numerical simulations corresponding to the experimental results in Fig. 3 of the main text, with three different detuning strengths,  $\Delta = 0, \sqrt{2}J$  and  $10J$ , are presented in Fig. S2 for both the  $\Phi = 0$  and  $\Phi = \pi$  cases.

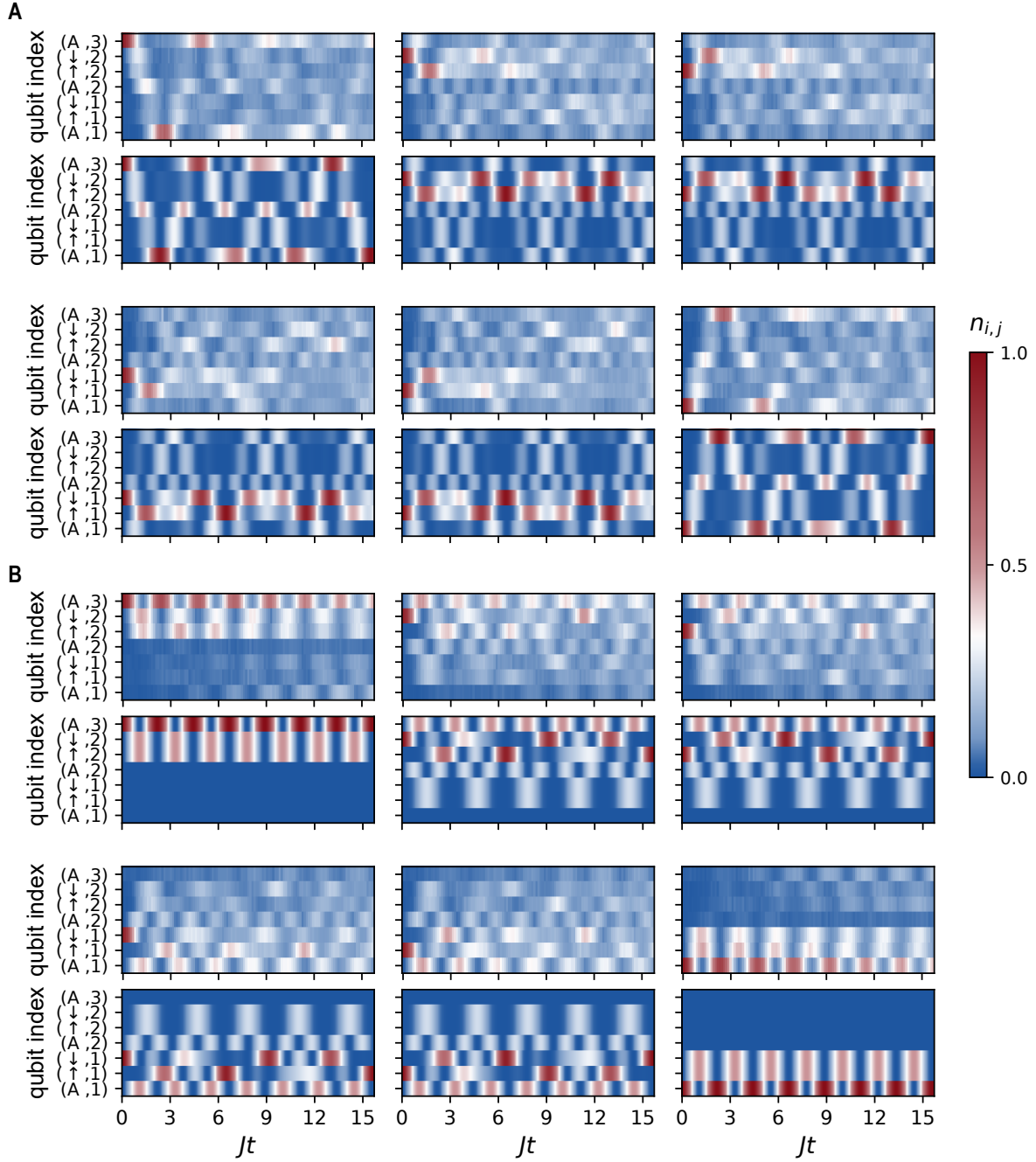


Fig. S1. **Characteristic dynamics of the rhombic array with coupler-assisted flux**  $\Phi = 0, \pi$ . **(A)**-**(B)** Measured population dynamics  $n_j$  versus normalized evolution time  $Jt$  for **(A)**  $\Phi = 0$  and **(B)**  $\Phi = \pi$ . The odd rows show the experimental results, while the even rows present the corresponding theoretical simulation results.

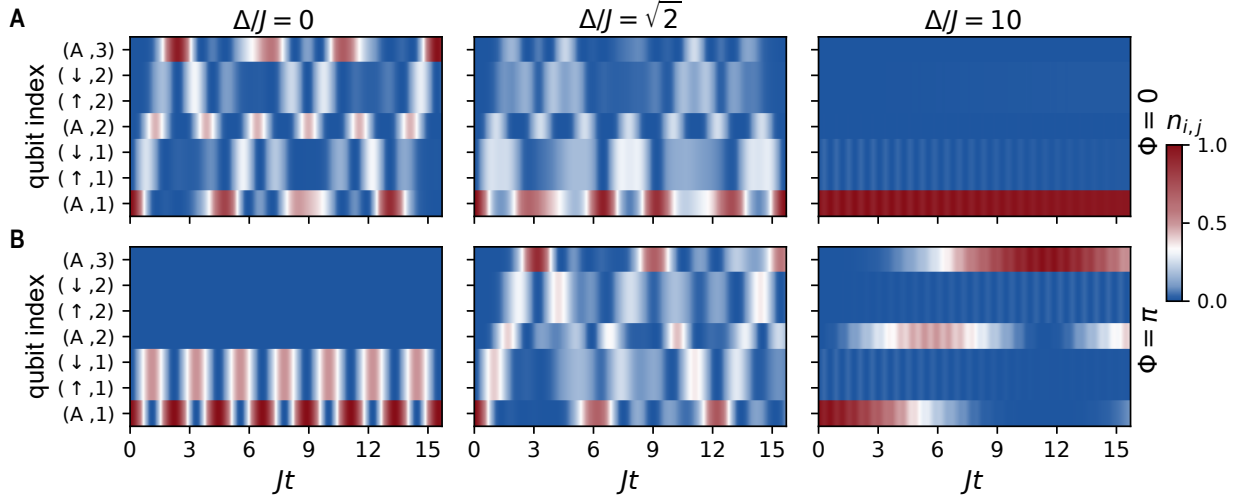


Fig. S2. Numerical simulation results of population dynamics  $n_j$  for (A)  $\Phi = 0$  and (B)  $\Phi = \pi$ , with anti-symmetric detuning  $\Delta = 0$ ,  $\sqrt{2}J$  and  $10J$ . The difference between the experimental results and the numerical simulations for the case with  $\Delta = 10J$  arises from the residual next-nearest-neighbor (NNN) couplings.

- 
- [1] S. Longhi, *Inverse Anderson transition in photonic cages*, *Opt. Lett.* **46**, 2872 (2021).
- [2] H. Li, Z. Dong, S. Longhi, Q. Liang, D. Xie, and B. Yan, *Aharonov-Bohm caging and inverse Anderson transition in ultracold atoms*, *Phys. Rev. Lett.* **129**, 220403 (2022).
- [3] J. G. C. Martinez, C. S. Chiu, B. M. Smitham, and A. A. Houck, *Flat-band localization and interaction-induced delocalization of photons*, *Sci. Adv.* **9**, 50 (2023).
- [4] I. T. Rosen, S. Muschinske, C. N. Barrett, D. A. Rower, R. Das, D. K. Kim, B. M. Niedzielski, M. Schuldt, K. Serniak, M. E. Schwartz, J. L. Yoder, J. A. Grover, and W. D. Oliver, *Flat-band (de)localization emulated with a superconducting qubit array*, *arXiv preprint*, [arXiv:2410.07878](https://arxiv.org/abs/2410.07878) (2024).
- [5] C. Danieli, A. Andreanov, T. Mithun, and S. Flach, *Nonlinear caging in all-bands-flat lattices*, *Phys. Rev. B* **104**, 085131 (2021).
- [6] V. M. Martinez Alvarez and M. D. Coutinho-Filho, *Edge states in trimer lattices*, *Phys. Rev. A* **99**, 013833 (2019).
- [7] A. Anastasiadis, G. Styliaris, R. Chaunsali, G. Theocharis, and F. K. Diakonov, *Bulk-edge correspondence in the trimer Su-Schrieffer-Heeger model*, *Phys. Rev. B* **106**, 085109 (2022).
- [8] F. Yan, P. Krantz, Y. Sung, M. Kjaergaard, D. L. Campbell, T. P. Orlando, S. Gustavsson, and W. D. Oliver, *Tunable coupling scheme for implementing high-fidelity two-qubit gates*, *Phys. Rev. Applied* **10**, 054062 (2018).
- [9] Y. Xu, J. Chu, J. Yuan, J. Qiu, Y. Zhou, L. Zhang, X. Tan, Y. Yu, S. Liu, J. Li, *et al.*, *High-fidelity, high-scalability two-qubit gate scheme for superconducting qubits*, *Phys. Rev. Lett.* **125**, 240503 (2020).
- [10] Y. Liang, C. Xie, Z. Guo, P. Huang, W. Huang, Y. Liu, J. Qiu, X. Sun, Z. Wang, X. Yang, *et al.*, *Dephasing-assisted diffusive dynamics in superconducting quantum circuits*, *arXiv preprint*, [arXiv:2411.15571](https://arxiv.org/abs/2411.15571) (2024).